

Statistical properties of dust far-infrared emission

M.-A. Miville-Deschénes^{1,2}, G. Lagache¹, F. Boulanger¹, and J.-L. Puget¹

¹ Institut d'Astrophysique Spatiale, Université Paris-Sud, Bât. 121, 91405, Orsay, France

² Canadian Institute for Theoretical Astrophysics, University of Toronto, 60 St. George Street, Toronto, ON, M5S 3H8, Canada

February 1, 2008

ABSTRACT

Context. Far-infrared dust emission has a self-similar structure which reveals the complex dynamical processes that shape the interstellar medium. The description of the statistical properties of this emission gives important constraints on the physics of the interstellar medium but it is also a useful way to estimate the contamination of diffuse interstellar emission in the cases where it is considered a nuisance.

Aims. The main goals of this analysis of the power spectrum and non-Gaussian properties of far-infrared dust emission are 1) to estimate the power spectrum of interstellar matter density in three dimensions, 2) to review and extend previous estimates of the cirrus noise due to dust emission and 3) to produce simulated dust emission maps that reproduce the observed statistical properties.

Methods. To estimate the statistical properties of dust emission we analyzed the power spectrum and wavelet decomposition of 100 μm IRIS data (an improved version of the IRAS data) over 55 % of the sky. The simulation of realistic infrared emission maps is based on modified Gaussian random fields.

Results. The main results are the following. 1) The cirrus noise level as a function of brightness has been previously overestimated. It is found to be proportional to $\langle I \rangle$ instead of $\langle I \rangle^{1.5}$, where $\langle I \rangle$ is the local average brightness at 100 μm . This scaling is in accordance with the fact that the brightness fluctuation level observed at a given angular scale on the sky is the sum of fluctuations of increasing amplitude with distance on the line of sight. 2) The spectral index of dust emission at scales between 5 arcmin and 12.5° is $\langle \gamma \rangle = -2.9$ on average but shows significant variations over the sky. Bright regions have systematically steeper power spectra than diffuse regions. 3) The skewness and kurtosis of brightness fluctuations is high, indicative of strong non-Gaussianity. Unlike the standard deviation of the fluctuations, the skewness and kurtosis do not depend significantly on brightness, except in bright regions ($> 10 \text{ MJy sr}^{-1}$) where they are systematically higher, probably due to contrasted structures related to star formation activity. 4) Based on our characterization of the 100 μm power spectrum we provide a prescription of the cirrus confusion noise as a function of wavelength and scale. 5) Finally we present a method based on a modification of Gaussian random fields to produce simulations of dust maps which reproduce the power spectrum and non-Gaussian properties of interstellar dust emission.

Key words. Methods: statistical – ISM: structure – Infrared: ISM: continuum – dust

1. Introduction

The interstellar medium emission shows fluctuations at all observable scales, revealing the self-similar nature of its density structure. The physical processes responsible for this self-similarity of the interstellar medium (ISM) structure is yet to be fully identified. It could be related to turbulent motions but also to chemical and thermal instabilities which trigger phase transitions and play an important role in shaping the medium.

Faced with the challenge to understand and characterize the great structural complexity of interstellar emission, astronomers have used several statistical tools (power spectrum, correlation and structure functions, wavelets, area-perimeter relation, principal component analysis,...) on several interstellar tracers : molecules (Falgarone et al., 1991; Hobson, 1992; Stutzki et al., 1998; Bensch et al., 2001; Brunt, 2003; Padoan et al., 2003), atomic hydrogen (Crovisier & Dickey, 1983; Green, 1993;

Stanimirovic et al., 1999; Stanimirovic & Lazarian, 2001; Dickey et al., 2001; Elmegreen et al., 2001; Miville-Deschénes et al., 2003a), extinction (Padoan et al., 2002; Padoan et al., 2006) or dust emission (Gautier et al., 1992; Abergel et al., 1996; Jewell, 2001; Ingalls et al., 2004).

The analysis of the results of these tools is made difficult by projection, and instrumental effects but also by the fact that no observation is a perfect tracer of the total gas column density. Several works have been dedicated to the understanding of these effects (Goldman, 2000; Elmegreen et al., 2001; Padoan et al., 2001; Miville-Deschénes et al., 2003b) and specifically on how one can retrieve the three-dimensional statistical properties of interstellar matter from astronomical observations. The recent theoretical progresses made in that area open interesting perspectives on the use of statistical tools to determine the three-dimensional structure of the gas and to identify privileged scales at which physical processes are important.

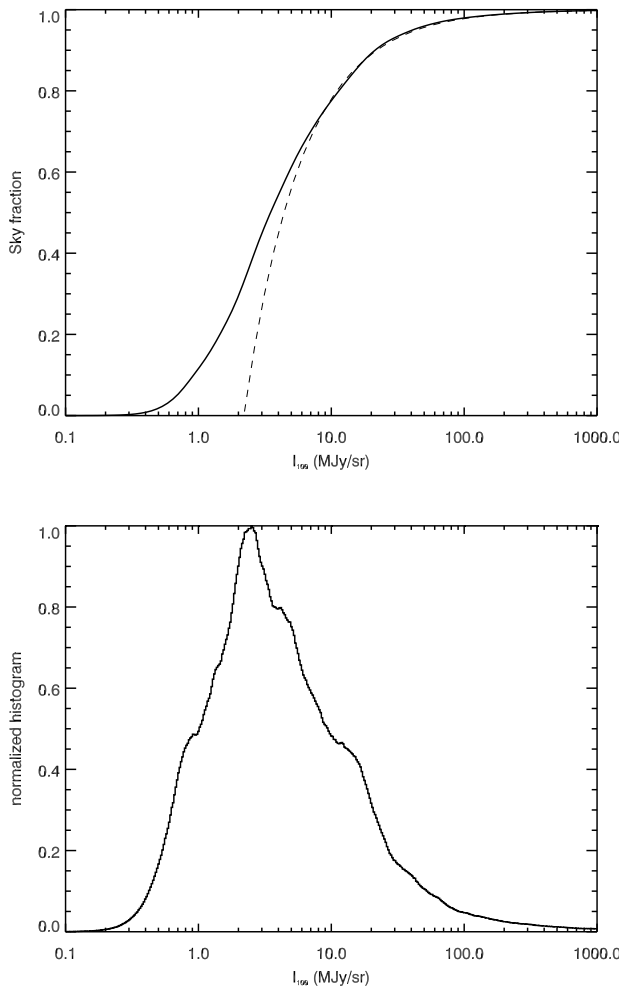


Fig. 1. **Top.** Cumulative histogram of $100 \mu\text{m}$ surface brightness over 98% of the sky (solid line): fraction of the sky with a brightness lower or equal to I_{100} . The dashed line represent what would be expected from a cylindrical disk (cosecant law). **Bottom.** Histogram of I_{100} brightness over the whole sky with bin scaled logarithmically. For both curves we used the IRIS data projected on the Healpix grid (equal area pixels - <http://healpix.jpl.nasa.gov>) with a pixel size of 1.7 arcmin ($\text{nside}=2048$). A background of 0.78 MJy sr^{-1} was removed from the data to take into account the cosmic infrared background and any zodiacal light residual (Hauser et al., 1998; Lagache et al., 2000).

The characterization of the statistical properties of the interstellar emission is relevant for the understanding of the physics of the ISM but is also of importance for studies where interstellar emission is a nuisance. This is the case of the study of pre-stellar cores in molecular clouds but also of the analysis of the Cosmic Microwave Background (CMB) and Cosmic Infrared Background (CIB) radiations. In these cases the interstellar emission is considered as a noise (the so-called “cirrus noise”) for which one needs a detailed statistical description in order to remove it and account for it in the error budget. In that respect the interstellar medium is a rather complex noise source due to its highly non-white and non-Gaussian brightness fluctuations.

$\langle I_{100} \rangle$	$16.18 \text{ MJy sr}^{-1}$
median I_{100}	3.49 MJy sr^{-1}
most probable I_{100}	2.51 MJy sr^{-1}
$< 0.1 \text{ MJy sr}^{-1}$	0.006%
$< 0.2 \text{ MJy sr}^{-1}$	0.06%
$< 0.5 \text{ MJy sr}^{-1}$	1.8%
$< 1.0 \text{ MJy sr}^{-1}$	11.6%
$< 2.0 \text{ MJy sr}^{-1}$	29.5%
$< 5.0 \text{ MJy sr}^{-1}$	61.1%
$< 10.0 \text{ MJy sr}^{-1}$	77.6%
$< 20.0 \text{ MJy sr}^{-1}$	89.2%
$< 50.0 \text{ MJy sr}^{-1}$	95.6%

Table 1. Average, median and most probable value of the $100 \mu\text{m}$ brightness over 98 % of the sky at an angular resolution of 4.3 arcminutes. The bottom portion of the table gives the fraction of the sky with brightness lower than the value given in the left column.

The present paper is a study of the power spectrum of interstellar dust emission at $100 \mu\text{m}$. The main goals are to use such analysis to put some constraints on the density structure of the interstellar medium but also to propose a caveat for estimation and simulation of cirrus noise. Gautier et al. (1992) showed that the power spectrum of the IRAS $100 \mu\text{m}$ emission is characterized by a power law $P(k) = A k^\gamma$ where the exponent $\gamma \sim -3$ is independent of the brightness. Moreover Gautier et al. (1992) showed that the normalisation factor of the power spectrum depends on the mean brightness $\langle I \rangle$ of the region considered, with $A \propto \langle I \rangle^3$. This study has been conducted on a relatively small number of regions and at a time where the instrumental response of IRAS was not well known. In this paper we would like to revisit the work of Gautier et al. (1992) by extending it to the whole sky and by taking advantage of the recent reprocessing of the ISSA plates by Miville-Deschénes & Lagache (2005).

In § 2 we present the data used in this analysis. The results of the power spectrum analysis and the implication on the ISM density structure are presented in § 3. An estimate of the cirrus noise level in the FIR-submm is provided in § 4 and a method to produce realistic dust emission maps is given in § 5.

2. The IRAS survey and IRIS

In 1983 the Infrared Astronomical Satellite (IRAS) has made a survey of 98% of the sky in four bands : 12, 25, 60 and $100 \mu\text{m}$. Since then this dataset has been used extensively in almost all area of astrophysics. In the early 90s the IRAS team released the IRAS Sky Survey Atlas, a set of 430 fields with better calibration. Each field is a $12.5^\circ \times 12.5^\circ$ image with a pixel size of $1.5' \times 1.5'$. Recently Miville-Deschénes & Lagache (2005) reprocessed the ISSA maps to correct for residual calibration defects and striping. This new set of ISSA plates, named IRIS, improves significantly the quality of the IRAS data by lowering the noise level and improving the photometry of the four bands. Our analysis is based on the $100 \mu\text{m}$ IRIS maps, available in native $12.5^\circ \times 12.5^\circ$ cartesian maps or in Healpix vector at <http://www.cita.utoronto.ca/~mamd/IRIS/>.

One important parameter of our analysis is the estimate of the instrumental noise contribution to the power

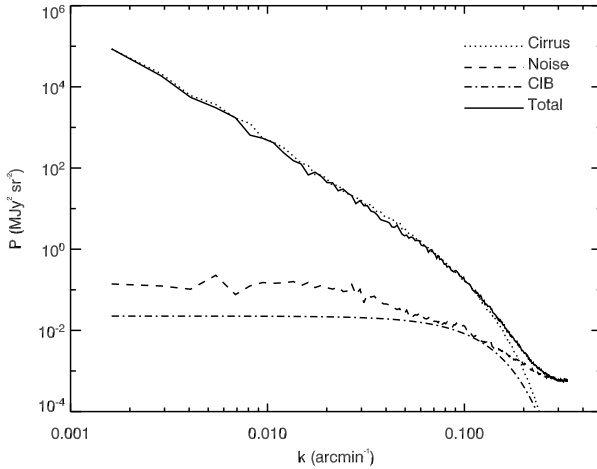


Fig. 2. Power spectrum of a typical IRIS map (point sources removed) with its associated noise power spectrum and the estimated CIB level (convolved by the IRAS beam). The power law at large scale (small k) is due to the Galactic dust emission. The cutoff at $k \sim 0.1 \text{ arcmin}^{-1}$ is due to the IRAS beam.

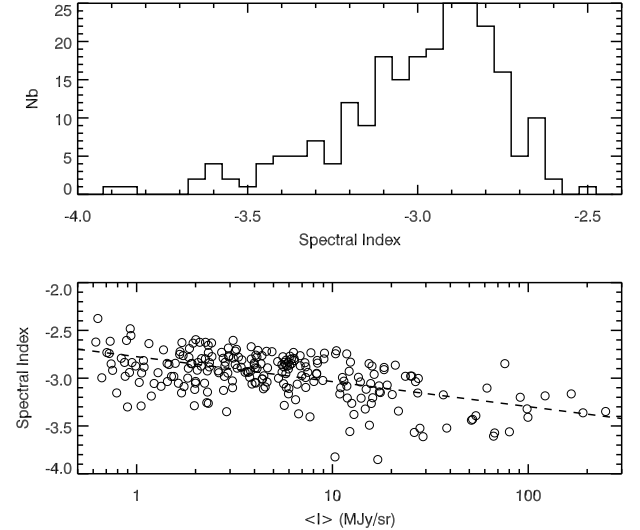


Fig. 3. Spectral index γ of the power spectrum for our sample. **Top.** Histogram of the spectral index values. Median is -2.93, average is -2.96 and standard deviation is 0.3. **Bottom.** Spectral index as a function of average $100 \mu\text{m}$ brightness (CIB and zodiacal light subtracted).

spectrum. We used only the IRIS maps for which we could compute the contribution of the noise. To do so we used the fact that the original ISSA plates are the combination of up to three HCON images. The power spectrum of the noise can be estimated by taking the power spectrum of the difference between two HCON images, as described in more details by Miville-Deschénes et al. (2002).

We selected only maps for which each pixel has been observed at least two times so that a noise map can be computed, which represent 236 maps (out of 430). Most maps of our sample have an average brightness $\langle I \rangle$ lower than 20 MJy sr^{-1} . This is representative of the whole sky statistics, as seen in Fig. 1 (see also Table 1) where the probability density function (PDF) and cumulative histogram of the $100 \mu\text{m}$ brightness (CIB and zodiacal light subtracted) over the whole sky is presented. This figure, together with Table 1, show that 90 % of the sky has a brightness lower or equal to 20 MJy sr^{-1} (or $N_H \lesssim 4 \times 10^{21} \text{ cm}^{-2}$ according to Lagache et al. (2000)). This simple statistics of $100 \mu\text{m}$ brightness reveals that there is less than 2 % of the sky with $N_H \lesssim 1 \times 10^{20} \text{ cm}^{-2}$.

3. Power spectrum analysis

The power spectrum has been extensively used in the analysis of image structure. Working in Fourier (or spherical harmonics) space offers considerable advantages; this formalism allows for the quadratic separation of uncorrelated sources in the image (e.g., noise and signal) and deconvolution of the instrumental function. In addition working in Fourier space facilitates the comparison with numerical simulations of turbulent flows.

3.1. Computation of the power spectrum

The power spectrum of an image $f(x, y)$ of Fourier Transform $\tilde{f}(k_x, k_y)$ is computed from the amplitude $A(k_x, k_y)$ defined as

$$A(k_x, k_y) = \tilde{f}(k_x, k_y) \tilde{f}^*(k_x, k_y) = |\tilde{f}(k_x, k_y)|^2. \quad (1)$$

The power spectrum $P(k)dk$ is an angular average of $A(k_x, k_y)$ between k and $k + dk$ where $k = \sqrt{k_x^2 + k_y^2}$. The method we use to compute the power spectrum is the one described by Miville-Deschénes et al. (2002). To minimize edges effects in Fourier space we apodize the image, from which the mean was removed, using a cosine taper of 15 pixels wide.

3.2. Contributions to the power spectrum

The main goal of our analysis is to characterize the power spectrum of the interstellar diffuse emission, but several astrophysical signals and artifacts may contribute to the power spectrum of the IRIS maps. The power spectrum $P(k)$ of the IRIS maps may be formalized by the following equation:

$$P(k) = B(k)(P_{ism}(k) + P_{sources}(k) + P_{cib}) + N(k) \quad (2)$$

where $B(k)$ is the effective beam of the IRIS maps (which includes the instrumental beam and the map making), $P_{ism}(k)$, $P_{sources}(k)$, $P_{cib}(k)$ and $N(k)$ are respectively the contributions of the interstellar medium, detected point sources, the unresolved CIB and the noise. All these contributions have to be estimated to characterize the interstellar component.

A typical power spectrum of a faint region of the sky is shown in Fig. 2. At large scales (low k), the power spectrum follows a power law Ak^γ ; this is the signature of the cirrus cloud emission (Gautier et al., 1992). At smaller scales,

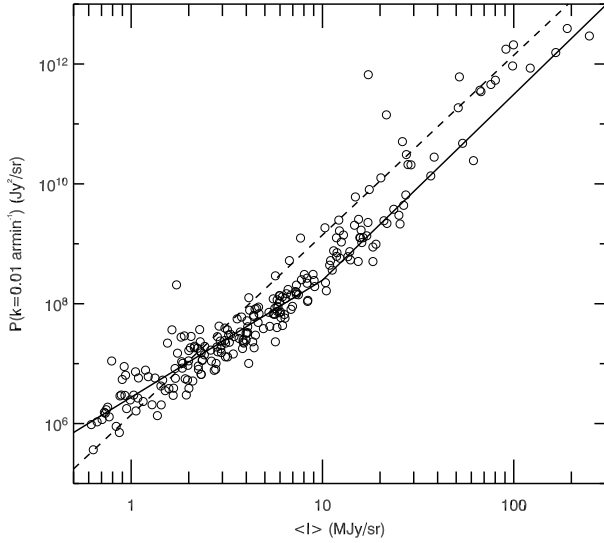


Fig. 4. Normalisation $P(0.01)$ of the power spectrum at 0.01 arcmin^{-1} of each map as a function of its mean $100 \mu\text{m}$ brightness. The solid line is our fit to the data (see Equations 5 and 6). The dashed line is the relation given by Gautier et al. (1992).

the power spectrum flattens due to the combination of the noise, point sources and the CIB. These three components have a power spectrum signature that is flatter than the cirrus emission.

As stated in § 2, the power spectrum of the noise is estimated by taking the power spectrum of the difference between two HCON images. An example of a noise map and its power spectrum is shown in Fig. 1 of Miville-Deschénes et al. (2002). The power spectrum of the noise is well described by a k^{-1} power spectrum over most of the k range.

To subtract the contribution of bright point sources we prefered to removed them directly in the IRIS maps prior to compute the power spectrum. To do so we used the point source extraction method described by Miville-Deschénes & Lagache (2005). For the CIB we assumed a flat power spectrum at the level determined by Miville-Deschénes et al. (2002) ($5.8 \times 10^3 \text{ Jy}^2 \text{ sr}^{-1}$ at $100 \mu\text{m}$). Like Miville-Deschénes et al. (2002) we made the assumption that the effective beam of the IRIS maps is Gaussian with a FWHM of 4.3 arcminutes.

3.3. Results

To obtain the spectral index of the dust emission in each IRIS map, we computed the power spectrum of the point source subtracted map and the power spectrum of the corresponding noise map. We then subtracted the noise power spectrum, divide the result by the Gaussian PSF and remove the CIB contribution.

Following what was done by Gautier et al. (1992) we have fitted the power spectrum of the Galactic emission in the range between $k = 0.004$ and $k = 0.08 \text{ arcmin}^{-1}$ using a power law:

$$P(k) = P_0 \left(\frac{k}{k_0} \right)^\gamma \quad (3)$$

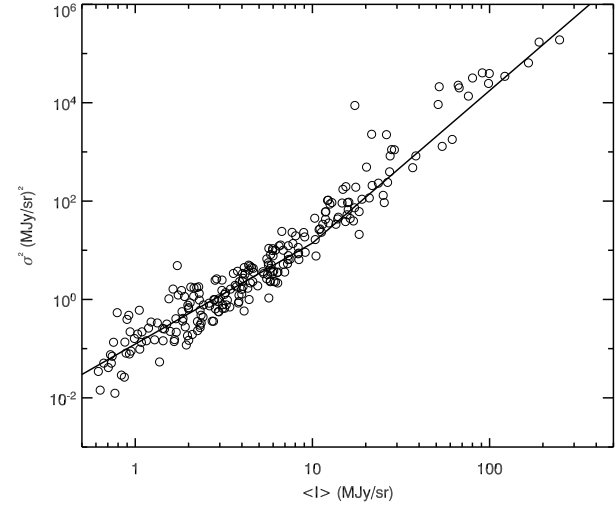


Fig. 5. Standard deviation as a function of the average interstellar brightness at $100 \mu\text{m}$ for each map of our sample. The noise level of each map and the CIB fluctuation level (0.09 MJy sr^{-1} - see Miville-Deschénes et al. (2002)) were removed quadratically from σ . The solid line represents the two regimes given by equations 7 and 8.

where P_0 is the power spectrum value at $k_0 = 0.01 \text{ arcmin}^{-1}$. The power spectrum of the interstellar emission is in general very well fitted by such a power law.

3.3.1. Spectral index

The compilation of the power spectrum spectral index measured on our sample of 236 maps is shown in Fig. 3. The most probable spectral index is $\gamma = -2.9 \pm 0.2$, in accordance with what was measured by Gautier et al. (1992). On the other hand, contrary to Gautier et al. (1992) who did their statistical analysis on only four regions, our larger sample allowed us to highlight a significant variation of the spectral index with the average brightness of the maps. Brighter regions on the sky tend to have a steeper power spectrum (see the lower panel of Fig. 3). The decrease of the spectral index with brightness can be approximated by:

$$\gamma = -0.26 \log_{10}(< I >) - 2.77, \quad (4)$$

where $< I >$ is the mean $100 \mu\text{m}$ brightness of the $12.5^\circ \times 12.5^\circ$ map.

3.3.2. Normalisation

Regarding the normalization of the power spectrum Gautier et al. (1992) estimated that $P_0 = 1.4 \times 10^6 < I >^3$, where $< I >$ is the mean $100 \mu\text{m}$ brightness at the 12.5° scale, given in MJy sr^{-1} , and P_0 is in $\text{Jy}^2 \text{ sr}^{-1}$. In Fig. 4 we present the variation of P_0 with $< I >$ for our sample, together with the relation of Gautier et al. (1992) (dashed line). The result of our analysis showed that the relation of Gautier et al. (1992) generally overestimates the fluctuation level at a given mean brightness. This discrepancy could be partly attributed to the fact that we used better calibrated IRAS data compare to the early IRAS product used by Gautier et al. (1992). On the other hand it is important to point out that the normalization relation given

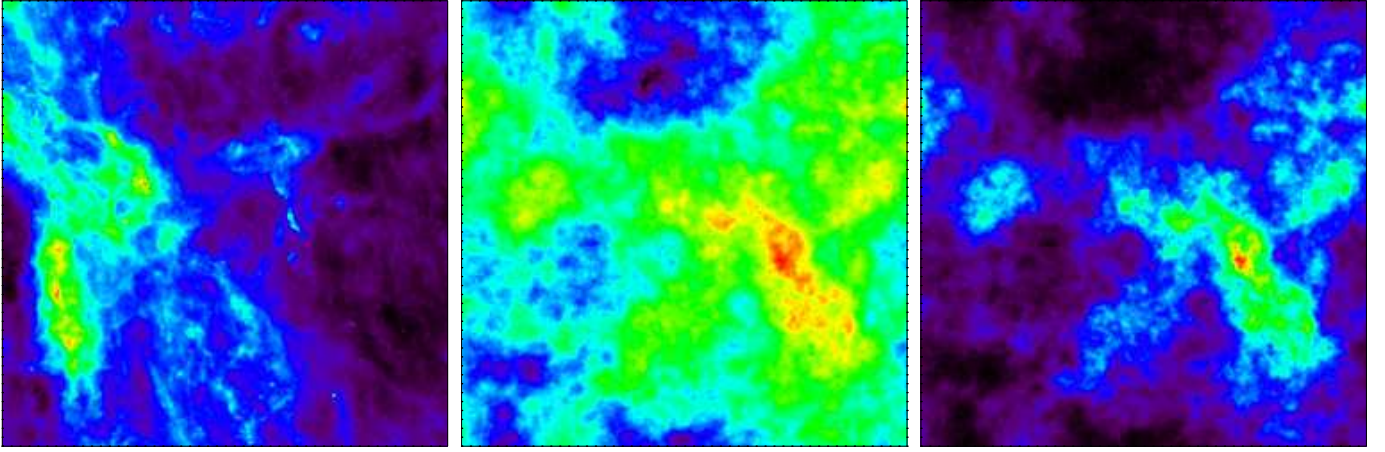


Fig. 6. **Left:** A typical IRIS map at 100 μm . **Center:** A classical fBm map with same power spectrum as the IRIS map shown on the left. This fBm has Gaussian brightness fluctuations at all scale and everywhere. **Right:** A modified version of the classical fBm with only positive values and the same average, standard deviation and skewness values as the IRIS map. The fBm has been modified in order to reproduce the $\sigma(I) \propto < I >$ relation which results in stronger brightness fluctuations in brighter regions.

by Gautier et al. (1992) is compatible with the fact that they used only two faint ($< I > \sim 4 \text{ MJy sr}^{-1}$) and two bright regions ($< I > \sim 30 \text{ MJy sr}^{-1}$).

Using a much larger sample than Gautier et al. (1992) we found that the normalization of the power spectrum is better described by two regimes (solid line in Fig. 4): on $\sim 80\%$ of the sky $P(0.01)$ is proportional to $< I >^{2.0 \pm 0.1}$ instead of $< I >^3$. For $< I > < 10 \text{ MJy sr}^{-1}$ we find

$$P(0.01) = 2.7 \times 10^6 < I >^{2.0 \pm 0.1}. \quad (5)$$

and for $< I > \geq 10 \text{ MJy sr}^{-1}$ we find

$$P(0.01) = 2.0 \times 10^5 < I >^{3.1 \pm 0.1}. \quad (6)$$

A similar trend was also observed by Jeong et al. (2005) using ISOPHOT observations (see their Fig. 12).

Another way of looking at the $P(0.01) - < I >$ relation is to plot the standard deviation σ_L^2 of each map as a function of $< I >$ (see Fig. 5). Here we made sure to remove quadratically the contribution of the instrumental noise and the CIB to each values of σ_L^2 . Like for the power spectrum normalisation, two regimes are apparent in the σ_L^2 vs $< I >$ relation with a transition around $< I > = 10 \text{ MJy sr}^{-1}$. Separating the data sample in two gives the following fits. for $< I > < 10 \text{ MJy sr}^{-1}$:

$$\sigma_L^2 = 0.12 < I >^{2.0 \pm 0.1} (\text{MJy}^2 \text{ sr}^{-2}) \quad (7)$$

and for $< I > \geq 10 \text{ MJy sr}^{-1}$

$$\sigma_L^2 = 0.011 < I >^{3.1 \pm 0.1} (\text{MJy}^2 \text{ sr}^{-2}) \quad (8)$$

3.4. Interpretation

3.4.1. Spectral index and density structure

Most spectral indexes measured here fall in the range between $\gamma = -3.6$ to $\gamma = -2.5$. This is compatible with what was found by Wright (1998) ($\gamma = -3$) in a power spectrum analysis of the DIRBE data at 60, 100, 140 and 240 μm on scales greater than 40 arcminutes. Other studies also

estimated the equivalent of the power spectrum spectral index of the 100 μm emission using the area-perimeter relation. Following Stutzki et al. (1998) there is a direct relation between the fractal dimension D deduced from the area-perimeter relation ($p \propto a^{D/2}$) and the spectral index γ of the power spectrum ($P \propto k^\gamma$):

$$\gamma = 2D - 6. \quad (9)$$

Bazell & Desert (1988) and Dickman et al. (1990) measured $D = 1.25 \pm 0.05$ (corresponding to $\gamma = -3.5 \pm 0.1$) for relatively bright regions at 100 μm ($\sim 10 \text{ MJy sr}^{-1}$). These values of γ are rather high (steep power spectrum) but not incompatible with our analysis. In a similar analysis on fainter regions Vogelaar & Wakker (1994) measured $D = 1.45 \pm 0.1$, corresponding to $\gamma = -3.1 \pm 0.2$ which is very similar to our results.

The interpretation of these results in terms of the density structure of the ISM and the comparison with what is deduced from gas tracers can only be done by considering a model for the 100 μm emission. At this wavelength the interstellar emission is dominated by the grey body emission from big dust grains at thermal equilibrium with the radiation field (Desert et al., 1990). For a given model of the composition of dust grain (Desert et al., 1990; Li & Draine, 2001) the conversion of 100 μm brightness to gas column density depends on the gas/dust mass ratio (known to be rather constant in the ISM) and on the big grain equilibrium temperature. The big grain equilibrium temperature is related to the local radiation field strength and spectrum which depends on the presence or not of nearby heating sources and on the extinction. Variation of the dust equilibrium temperature can also occur locally due to variation of the grain structure which can affect their emissivity¹.

In diffuse regions of the sky at high Galactic latitudes, far from star-forming regions, clouds are optically

¹ Aggregation of small dust particles on bigger grains can increase significantly their area / mass ratio which leads to a more efficient cooling of the grains. See Stepnik et al. (2003) for a striking example of this effect.

thin to stellar radiation, and the radiation field is uniform which result in very limited variations of dust equilibrium temperature. Localised variations of the dust grain temperature were observed in cirrus clouds (Bernard et al., 1999), but overall several studies (Boulanger & Péault, 1988; Boulanger et al., 1996) showed a strong correlation between the 100 μm micron and the hydrogen column density which is in favor of a rather uniform gas/dust ratio and limited variations of the dust temperature. Based on these results we believe that the 100 μm micron can not be used as a perfect surrogate for gas column density but overall it does not introduce a systematic bias in the determination of the column density power spectrum. In this context, and considering that the power spectrum of the column density gives directly the power spectrum of the density structure (Miville-Deschénes et al., 2003b), we consider that the γ values measured here in the diffuse regions (for $\langle I \rangle < 10 \text{ MJy sr}^{-1}$) are typical of the spectral index of the density field in three dimensions in the solar neighborhood.

In bright regions ($\langle I \rangle > 10 \text{ MJy sr}^{-1}$) the power spectrum is observed to be significantly steeper (Fig 3). A steepening of the power spectrum with brightness was also found by Kiss et al. (2003) on 90-200 μm ISOPHOT observations. We observed that this steepening coincides with a departure from the $\sigma \propto \langle I \rangle$ relation (see Fig. 4) and a systematic increase of the skewness and kurtosis of the brightness fluctuations (see Fig. 11). This variation of γ with $\langle I \rangle$ might reflect, at least in part, local variations of the density power spectrum. It could also be attributed to the effect of gravity or anisotropic radiation fields which would both increase the large scale coherence (like in star forming regions or at Galactic scale in the plane) and therefore steepen the power spectrum of the 100 μm emission. The effect of extinction in these parts of the sky will also induce important dust temperature variations which will affect the power spectrum. These effects will certainly have an impact on the observed brightness fluctuations and make the interpretation of the power spectrum difficult.

To compare the results obtained here with statistical analysis of gas emission, it is important to point out that the 100 μm emission traces all the interstellar components: atomic, molecular and ionized gas. Gas observations (21 cm and CO) showed that diffuse and dense gas have different density structure. In general regions of cold and dense gas have stronger small scale fluctuations (and therefore a flatter density power spectrum - see for instance Stutzki et al. (1998) who measured $\gamma = -2.8$ on CO observations of the Polaris flare, a dense cirrus cloud with a significant fraction of molecular gas) than regions of diffuse gas (Miville-Deschénes et al. (2003a) measured $\gamma = -3.6 \pm 0.2$ on 21 cm observations of a diffuse cirrus cloud). This behavior seems also in accordance with numerical simulations (see Audit & Hennebelle (2005) for instance).

This could reflect the fact that molecular tracers like CO reveal only the density structure of dense regions and miss the more diffuse and large scale structure of molecular clouds. In that respect dust emission would be a more reliable tracer of the global density structure of the ISM as the observed spectral index at 100 μm is a weighted mean of the various contributions from dense and diffuse media on the line of sight. One striking example of that comes from the direct comparison of infrared and 21 cm emission in high-latitude clouds where dust emission usually shows stronger brightness fluctuations at small scale than HI, this

being attributed to the presence of localized molecular regions (see for instance Joncas et al. (1992)).

3.4.2. The $\sigma \propto \langle I \rangle$ relation

Here we would like to propose one interpretation for the scaling of the power spectrum normalization $P(0.01)$ (or equivalently the brightness standard deviation σ_L) with average brightness $\langle I \rangle$ (equations 5 and 7).

Lets consider a three-dimensional scalar field ϵ , which could be a dust emissivity field, of size $L \times L$ on the plane of the sky and of depth H . In the case of constant dust temperature and neglecting opacity effects, the projection of this 3D field on 2D would correspond to a dust emission map:

$$I(x, y) = \int_0^H \epsilon(x, y, z) dz. \quad (10)$$

What would be the relation between the average and standard deviation of the projected brightness for such a field ? The average brightness of the dust map is simply

$$\langle I \rangle = \langle \epsilon \rangle H \quad (11)$$

where $\langle \epsilon \rangle$ is the volume averaged of ϵ .

On the other hand to compute the standard deviation of the dust map (σ_I) one should consider that brightness fluctuations are added quadratically along the line of sight. Each slice dz of the cube contributes $\sigma_\epsilon^2 dz$ to σ_I^2 :

$$\sigma_I^2 = \int_0^H \sigma_\epsilon^2 dz = \sigma_\epsilon^2 H. \quad (12)$$

Combined with Eq. 11 this leads to

$$\sigma_I^2 \propto \langle I \rangle \quad (13)$$

which is not what is observed.

Cartesian coordinates used in the previous demonstration is in fact not a realistic representation when it comes to estimate σ_I . In fact, with the increase of the depth of the line of sight z , a given angular scale θ on the sky corresponds to increasing physical size $l : \tan(\theta) = l/z$.

In the integral of Eq. 12 we made the assumption that σ_ϵ is the standard deviation at scale L . In fact we should have taken into account that σ_ϵ varies with z . For a power spectrum following a power law ($P(k) \propto k^\gamma$) the variance of brightness fluctuations as a function of scale l is (Brunt & Heyer, 2002):

$$\sigma_l \propto l^{-\gamma/2-1}. \quad (14)$$

Therefore we can rewrite Eq. 12

$$\sigma_I^2(\theta) \propto \int_0^H l^{-\gamma-2} dz = \int_0^H (\tan(\theta)z)^{-\gamma-2} dz \quad (15)$$

which leads to

$$\begin{aligned} \sigma_I^2(\theta) &\propto \tan(\theta)^{-\gamma-2} H^{-\gamma-1} \\ &\propto \tan(\theta)^{-\gamma-2} \langle I \rangle^{-\gamma-1}. \end{aligned} \quad (16)$$

There are two important results to extract from the previous equation. First the fact that we observed structure of increasing physical size with z at a given angular scale θ does not modify the slope of the power law for $\theta \lesssim 25^\circ$:

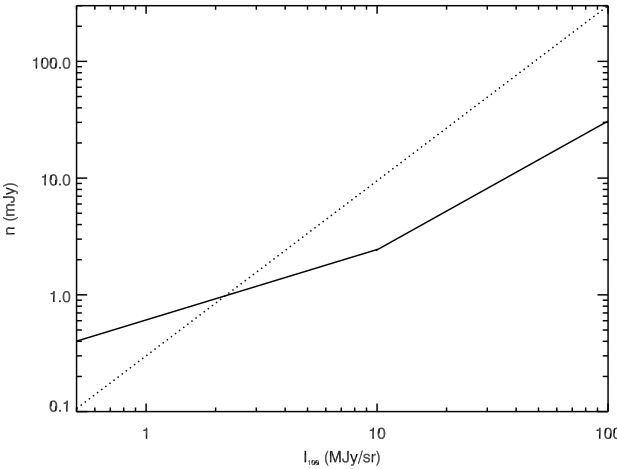


Fig. 7. Cirrus noise at 100 μm for a 1m diffraction limited telescope (FWHM=33 arcseconds) as a function of I_{100} brightness. Solid line is our estimate and dotted line is the estimate of Helou & Beichman (1990).

both $\sigma_I(\theta)$ and $\sigma_\epsilon(l)$ have the same spectral index $(\gamma-2)/2$. Secondly the dependence of σ_I on $\langle I \rangle$ is now related to the spectral index γ . For a typical value of $\gamma = -3$ we obtain $\sigma_I^2 \propto \langle I \rangle^2$ which is exactly the observed relation for $\langle I \rangle < 10 \text{ MJy sr}^{-1}$.

For larger $\langle I \rangle$ the departure from a simple $\sigma_I^2 \propto \langle I \rangle^2$ can be explained partly because the spectral index γ decreases but most of all it is important to notice that brightness fluctuations become highly non-Gaussian (high skewness and kurtosis - see Fig. 11). In this regime the standard deviation becomes significantly affected by non-Gaussian fluctuations which could be related to localized star forming regions in the image.

4. Cirrus noise

In this section we use the properties of the power spectrum of 100 μm emission to estimate the level of cirrus confusion noise of dust emission.

4.1. Brightness fluctuations

To estimate the level of fluctuations as a function of scale and brightness it is convenient to use the real-space representation given by Eq. 14, as opposed to a Fourier one. Using the value of σ_l measured at $l = L = 12.5^\circ$ (see equations 7 and 8) we can normalize Eq. 14 and estimate the level of brightness fluctuation of interstellar dust (in MJy sr^{-1}) at scale l (in degree) and wavelength λ . For the two regimes identified in this study (lower and higher than $\langle I_{100} \rangle = 10 \text{ MJy sr}^{-1}$) we have the following relations:

$$\sigma_{l,\lambda}^{low} = 0.35 \langle I_{100} \rangle \frac{I_\lambda}{I_{100}} \left(\frac{l}{12.5^\circ} \right)^{-\gamma/2-1} \quad (17)$$

and

$$\sigma_{l,\lambda}^{high} = 0.10 \langle I_{100} \rangle^{1.5} \frac{I_\lambda}{I_{100}} \left(\frac{l}{12.5^\circ} \right)^{-\gamma/2-1}. \quad (18)$$

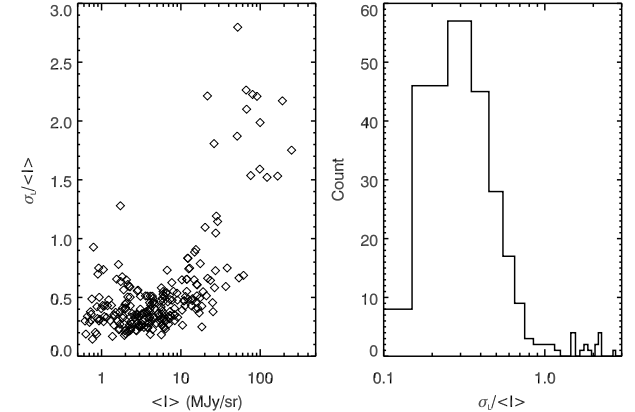


Fig. 8. Contrast of interstellar emission: the standard deviation σ_L is the standard deviation of interstellar fluctuations at the 12° scale. **Left:** Contrast values as a function of average brightness. **Right:** Histogram of contrast values. According to Eq. 7, the contrast is close to constant for $\langle I \rangle$ lower than 10 MJy sr^{-1} . Outliers at low brightness corresponds to regions where there are bright structures on a very low level background, like the Magellanic Clouds.

where $\langle I_{100} \rangle$ is in MJy sr^{-1} , γ is given by Eq. 4 and I_λ/I_{100} is an estimate of the dust brightness ratio at wavelength λ and 100 μm . Such ratio can be estimated using a grey body model like the one of Desert et al. (1990)

$$\frac{I_\lambda}{I_{100}} = \frac{B_\nu(T_d)}{B_{100}(T_d)} \left(\frac{\lambda}{100 \mu\text{m}} \right)^{-\beta} \quad (19)$$

where $B_\nu(T_d)$ is the Planck function at grain temperature T_d and β is the dust emissivity index. Typical values in the diffuse ISM for the dust temperature T_d and emissivity index β are $T_d = 17.5 \text{ K}$ and $\beta = 2$. In the sub-millimeter and millimeter ranges the dust emission departs from this simple model and one might want to use a combination of two dust components (see Finkbeiner et al. (1999) for an example of such model).

4.2. Noise per beam

Equations 17 and 18 give the surface brightness fluctuation level of dust at any scale, brightness and wavelength. One useful specific case to consider is the contribution of cirrus noise at the scale of an instrument beam, to estimate the effective point source detection level for instance. Following Helou & Beichman (1990) and Gautier et al. (1992) we consider the cirrus noise level at a scale two times the beam size b (i.e., $l = 2b$, where b is the beam FWHM). This noise level (in mJy/beam) at wavelength λ is simply

$$n_\lambda = 10^9 \sigma_{2b,\lambda} \Omega \quad (20)$$

where Ω is the beam in steradian

$$\Omega = \pi \left(\frac{b}{2} \right)^2 \left(\frac{\pi}{180} \right)^2 \quad (21)$$

and b is in degrees. The cirrus noise in mJy/beam is then given by

$$n_\lambda^{low} = 3.3 \times 10^6 \langle I_{100} \rangle \frac{I_\lambda}{I_{100}} (0.16 b)^{-\gamma/2+1} \quad (22)$$

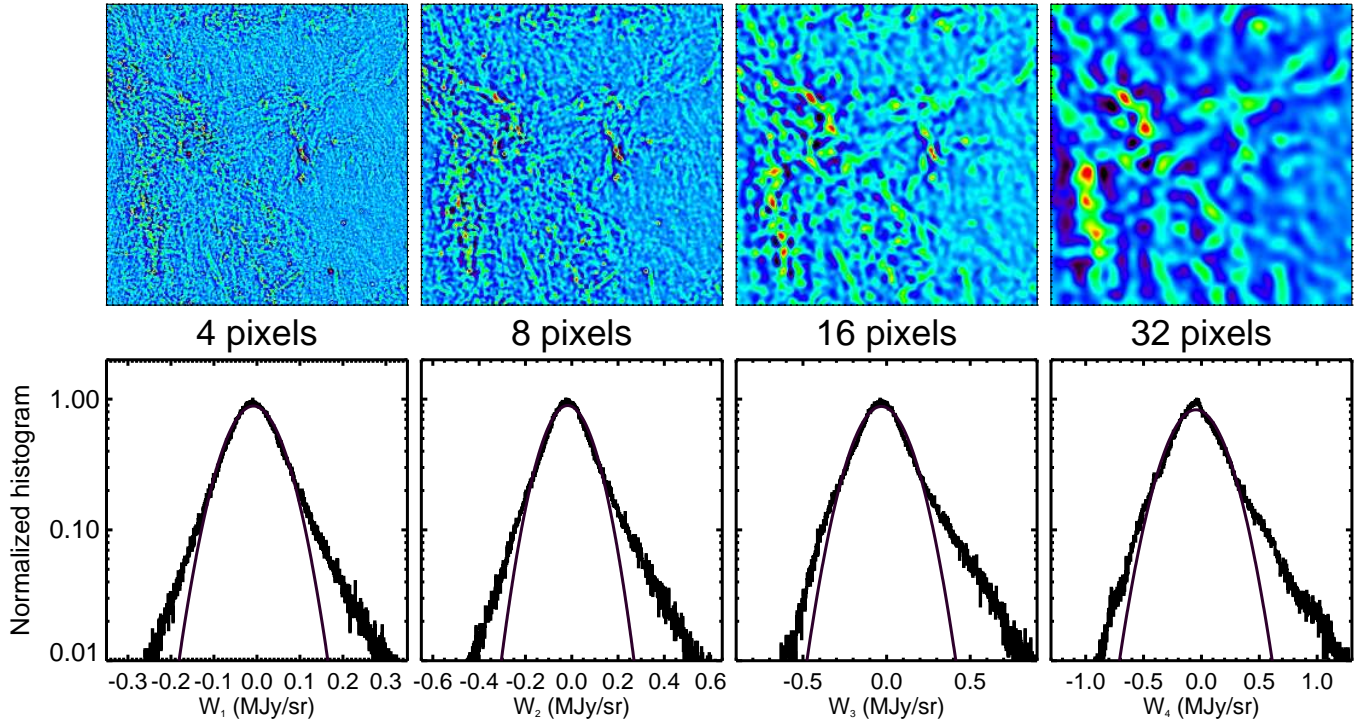


Fig. 9. Wavelet decomposition of the IRIS map shown in Fig. 6-left. **Top:** wavelet coefficients map at scales 4, 8, 16 and 32 pixels (1 pixel=1.5'). **Bottom:** Histogram of the wavelet coefficients in linear-log. A Gaussian fit to the histogram is superposed highlighting the non-Gaussian behavior.

and

$$n_{\lambda}^{high} = 1.0 \times 10^6 < I_{100} >^{1.5} \frac{I_{\lambda}}{I_{100}} (0.16 b)^{-\gamma/2+1} \quad (23)$$

where γ is still given by Eq. 4.

These relations can be compared with the prescription of Helou & Beichman (1990) often used to estimate cirrus confusion noise. These authors considered the situation where the beam of the instrument is given by the diffraction limit of a telescope of diameter D . In this case $b = (1.6\lambda/D)(180/\pi)$.

The comparison between our estimate of the cirrus noise and the one given by Helou & Beichman (1990) for a 1m telescope at 100 μ m is shown in Fig 7. The difference is important in several aspects. First at low brightness the slopes of $n(I_{100})$ are very different, due to the $\sigma \propto < I >$ regime revealed in our study. The change of slope has the implication that our estimate of the cirrus noise in low brightness regions is much higher. This is also due to the flattening of the power spectrum index γ at low brightness. On the other hand our cirrus noise estimate is much lower than the estimate of Helou & Beichman (1990) at large brightness. This effect is caused by the fact that we observe steeper power spectra in bright regions. Therefore the brightness fluctuations are much smaller when extrapolated to small scale.

4.3. Limitation

The prescriptions given here to estimate the level of cirrus noise is only indicative. It would be strictly correct for a

Gaussian field which is not the case of interstellar emission. As it will be described in more details in the next section, dust emission has non-Gaussian brightness fluctuations at all scales. For the sake of data interpretation, confusion estimate or tests of component separation algorithms (including point source extraction) it is useful to produce realistic simulations of dust emission maps with proper non-Gaussian properties. It is the topic of the next section.

5. Construction of artificial dust emission maps

5.1. Fractional Brownian motion

Fractional Brownian motions (fBm, also known as Gaussian random fields) are often used to simulate interstellar emission (e.g., Stutzki et al., 1998; Miville-Deschénes et al., 2003b). By construction such objects can reproduce the power spectrum of any image, with the limitation that its phase is random. A comparison of a typical IRIS map and a fBm with the same power spectrum is given in Fig. 6. The fBm reproduces well the self-similar structure of the interstellar emission. On the other hand the fBm seems smoother and less contrasted than the observation.

Because of the Gaussian nature of their fluctuations, fBms with positive values only can't have a large contrast. If we define the contrast of a map I as $C_I = \sigma(I)/< I >$, positive fBms are restricted to $C_I \lesssim 1/3$ as the average $< I >$ needs to be greater than 3σ to have only positive values². This can be compared with the contrast of real

² or equivalently that 99 % of the values are between $< I > - 3\sigma$ and $< I > + 3\sigma$.

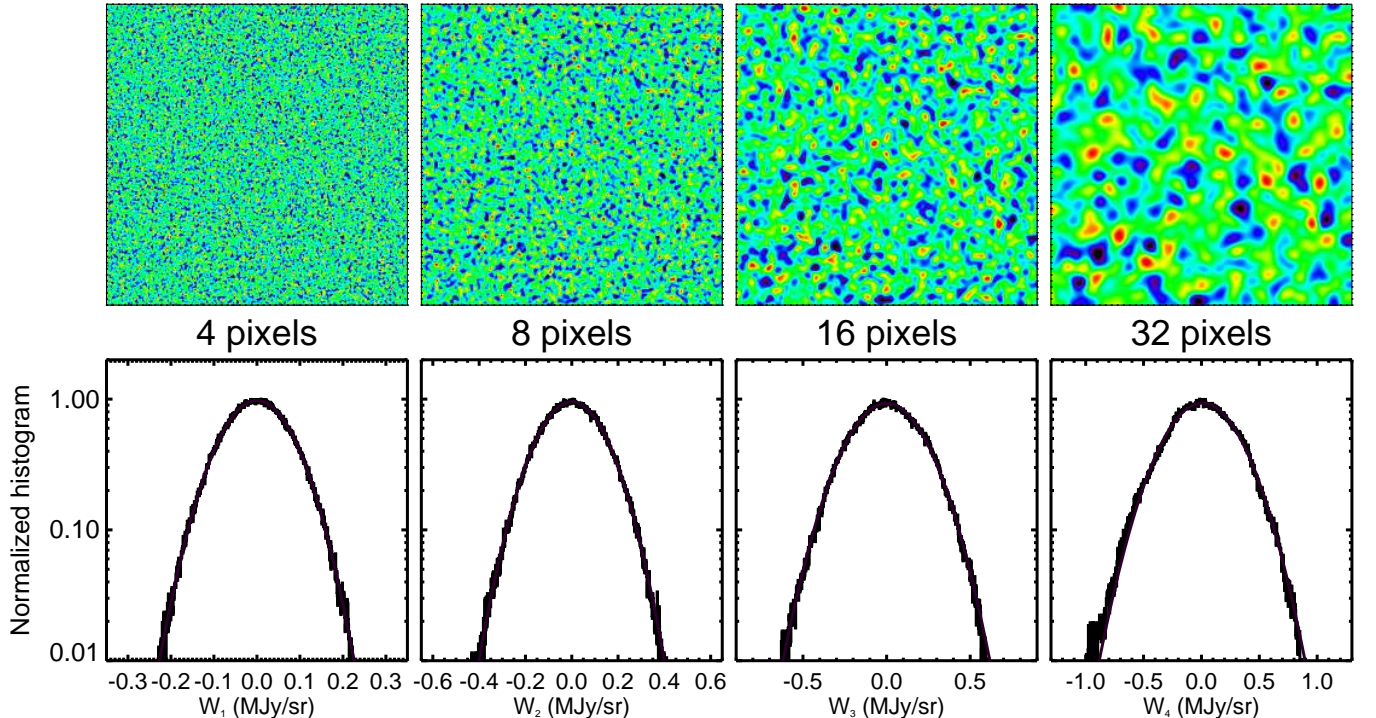


Fig. 10. Wavelet decomposition of the classical fBm map shown in Fig. 6-center. See Fig. 9 for details.

IRIS map given in Fig. 8, where we used $\sigma(I) = \sigma_L$ (i.e., the standard deviation at a scale of 12.5°). The median contrast is 0.3 which indicate the limitation of the use of fBms used to simulate realistic infrared dust maps. In addition one would notice that the contrast increases significantly with brightness and especially for $\langle I \rangle$ greater than 10 MJy sr^{-1} , in accordance with equations 7 and 8. In addition, C_I will increase with scale as $\sigma(I)$ depends on scale (according to Eq. 14) but not $\langle I \rangle$ (at high Galactic latitude). Based only on the contrast, the use of fBm becomes limited to small (a few degrees) and faint regions of the sky.

5.2. Wavelet decomposition

Apart from the global contrast limitation, there is a fundamental difference between fBms and observations which is related to the non-Gaussian properties of the interstellar emission. The brightness fluctuations seen in infrared dust maps show contrasted structures, often filaments, that reflect their non-Gaussian nature. Using a wavelet decomposition of $100 \mu\text{m}$ maps, Jewell (2001) showed clearly that, contrary to random-phase realisations, the histograms of brightness fluctuations at a given scale are highly non-Gaussian. Abergel et al. (1996) and Aghanim et al. (2003) gave also striking examples of that. Wavelet transforms are powerful tools to study the statistical moments higher than two and estimate the non-Gaussian properties of images (Aghanim et al., 2003). They complement the power spectrum analysis which gives only the variation of the second moment - the standard deviation - with scale.

To illustrate that we present in figures 9 and 10 the wavelet decomposition obtained using the “a trou” algorithm (Starck & Murtagh, 1998) for the IRIS and fBm

maps of Fig. 6. As expected the distribution of brightness fluctuations at a given scale are Gaussian for fBms (see Fig. 10). On the other hand the distribution of wavelet coefficients of an IRIS map (see Fig. 9) follows an asymmetrical distribution with exponential wings, which results in significant skewness and kurtosis.

In Fig. 11 are compiled the skewness and kurtosis of the wavelet coefficients found for all 236 maps of our sample, for scales from $l = 4$ pixels (12 arcmin) to 32 pixels (48 arcmin). There is a not a strong correlation of the skewness and kurtosis with brightness, unlike for the standard deviation (Fig. 5). There is a slight increase of skewness and kurtosis at small scale and low brightness that should be attributed to noise and CIB³. On the other hand one would note a sharp increase of the skewness and kurtosis for $\langle I \rangle > 10 \text{ MJy sr}^{-1}$.

Finally, apart from the global difference of the wavelet coefficient distribution between fBms and observations, one would notice that brightness fluctuations at a given scale in the IRIS map are generally greater in bright regions of the map, contrary to the fBm where the amplitude of fluctuations at a given scale is independent of position. This just reflects the fact that brightness fluctuations are generally stronger in bright region, in accordance with equations 7 and 8. By construction fBms do not behave like that; the amplitude of fluctuations is uniform and independant of local variations of the average brightness.

³ Both processes being more Gaussian than the interstellar emission they have the effect of lowering the skewness and kurtosis mostly. This effect is more important at small scale and low brightness where the noise and CIB fluctuations are stronger with respect to interstellar fluctuations.

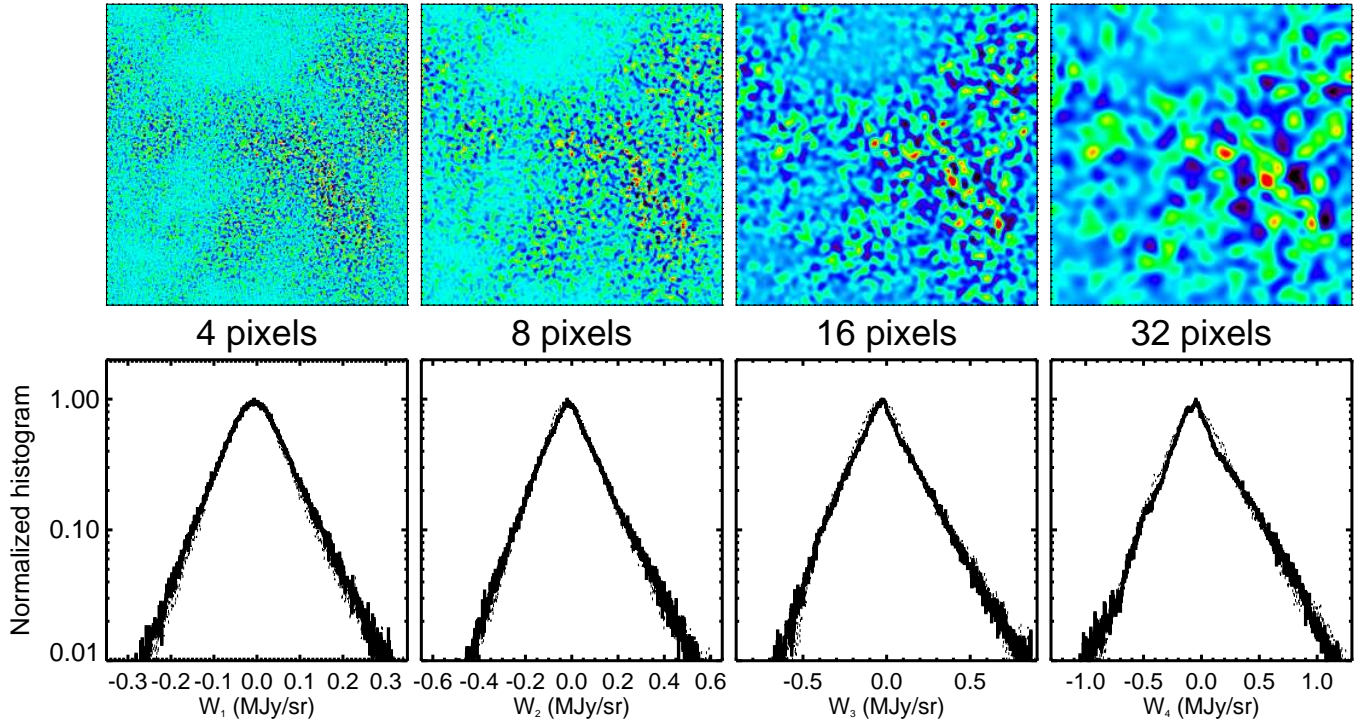


Fig. 12. Wavelet decomposition of the modified fBm map shown in Fig. 6-right. See Fig. 9 for details. The histogram of the wavelet coefficients of the IRIS map are over plotted (dots) showing how well the modified fBm reproduces the observed statistics.

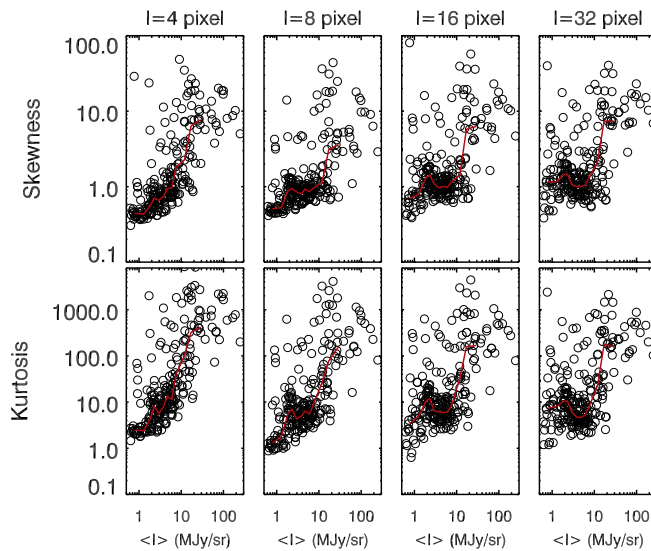


Fig. 11. Skewness (top) and Kurtosis (bottom) of the wavelet coefficients from $l=4$ to 32 pixels for each IRIS map of our sample. The solid red line is the median in a bin 20 values sorted by increasing $\langle I \rangle$.

5.3. Non-Gaussian fBm

In this section we propose a method to modify fBms such that they better reproduce the statistical properties of the infrared emission. We want to produce simulations of dust

emission maps that would satisfy a given number of assumptions:

1. Positive values only
2. Power spectrum following a power law : $P(k) = Ak^\gamma$
3. Greater brightness fluctuations in bright regions (following $\sigma \propto \langle I \rangle$).

Several attempts have been made to generate non-Gaussian maps, especially to produce non-Gaussian realizations of the Cosmic Microwave Background (CMB) (Vio et al., 2001, 2002; Rocha et al., 2005). In general these methods involve a modification of a Gaussian realization but they don't comply with all our requirements. Especially in the context of the CMB there is no need to produce maps with only positive values and to have stronger brightness fluctuations in bright regions.

Here is how we proceeded to construct a non-Gaussian fBm map with the same statistical properties as an IRIS map I and with only positive values. The method presented here is similar to the one used by Elmegreen (2002); Brunt & Heyer (2002). First we generate a classical fBm F with same standard deviation as map I . We add an offset to force all values to be positive and to be as close as possible to the average of I . We then create a modified fBm F' such that:

$$F' = AF^\psi + C \quad (24)$$

and such that F' has the same average, standard deviation and skewness than I and only positive values. The parameters A , ψ and C are thus constrained iteratively so to match the first three statistical moments of the map I . Such a

modified fBm is shown in Fig. 6 and its wavelet decomposition in Fig. 12. The effect of the exponent ψ is to produce greater fluctuations in bright regions, in accordance with the observations. The wavelet decomposition is quite illustrative in that respect. In particular the histograms of wavelet coefficients are almost impossible to discriminate from the ones of the IRIS map.

The key parameter in this transformation is ψ which control the amount of non-Gaussianity introduced in the map. We did such a simulation for each of the 236 maps of our sample and the results are summarized in Fig. 13. One would note the scaling of ψ with skewness χ , which clearly indicate the impact of that parameter on the non-Gaussianity of the map. The median value of ψ is ~ 2 (see Fig. 13).

Even though it reproduces very well several statistical properties of the observed emission, it is important to note that one important limitation of this method is that it produces only isotropic fluctuations and failed to reproduce to filamentary structure of the ISM.

5.4. Extend an image to smaller scales

To estimate the capabilities and performances of some instruments at observing diffuse interstellar emission it is often needed to extrapolate low resolution observations to smaller angular scales. One example of that would be the estimate of the diffuse emission structure that will be observed at a scale of 8 arcsec by Herschel-PACS given the IRAS data at 5 arcmin resolution. In this context it is useful to produce constrained realisations of the interstellar diffuse emission based on low resolution observations. The statistical analysis presented here provides a theoretical basis ($\sigma \propto \langle I \rangle$) on which to add small scales using larger scale informations.

Given a low resolution map I_0 characterized by a beam B_0 , a higher resolution I_1 of beam B_1 can be computed using the following method:

$$I_1 = I_0 + A (B_1 \otimes F - B_0 \otimes F) I_0^\psi + C \quad (25)$$

where F is a classical positive fBm map, and A , ψ and C are determined as described in the previous section. In the previous equation the difference $(B_1 \otimes F - B_0 \otimes F)$ extends the structure up to the higher resolution beam B_1 . The modulation of the small scale fluctuations by I_0^ψ assures that they follow the $\sigma \propto \langle I \rangle$ relation.

6. Conclusion

In this paper we presented an analysis of the power spectrum and wavelet decomposition of the IRIS/IRAS 100 μm emission over 55 % of the sky. The main goals of this work were 1) to review and extend the study of Gautier et al. (1992) using better calibrated IRAS maps, estimates of the noise and CIB contributions and a larger sample, 2) provide a more precise prescription for cirrus noise and 3) suggest a technique to simulate dust emission map with proper statistical properties.

We found an average spectral index ($\langle \gamma \rangle = -2.9 \pm 0.2$) compatible with Gautier et al. (1992) ($\gamma = -3$) but with a significant variation from $\gamma = -3.6$ to $\gamma = -2.5$. Considering that 100 μm emission is a relatively reliable tracer of column density in faint regions, these values of γ

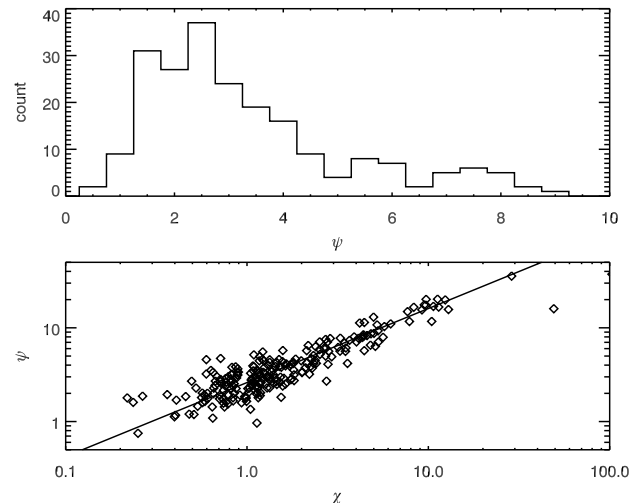


Fig. 13. **Top:** Histogram of all the exponent ψ used to simulate realistic fBm for each IRIS map of our sample. **Bottom:** Exponent ψ as a function of the skewness χ of each IRIS map. The straight line is $\psi = 2.6 \chi^{0.8}$.

should be representative of the spectral index of density in three dimensions in the local interstellar medium. The comparison with other tracers leads to the conclusion that there is most probably a significant contribution from cold gas to the brightness fluctuations observed. We also found a slight variation of γ with $\langle I \rangle$ which could be explained by the impact of gravity or spatial variations of dust temperature in star forming regions.

We also found that the amplitude of the brightness fluctuations were generally overestimated by Gautier et al. (1992). In regions with a 100 μm average brightness $\langle I \rangle$ lower than 10 MJy sr^{-1} the brightness fluctuation level is proportional to $\langle I \rangle$ and not $\langle I \rangle^{1.5}$ as stated by Gautier et al. (1992). We showed that this behavior can be explained by the fact that the brightness fluctuation level observed at a given angular size on the sky is the sum of fluctuations of increasing amplitude with distance.

This detailed description of the power spectrum properties of the 100 μm emission allowed us to determine a new prescription of the cirrus confusion noise in the far-infrared and sub-millimeter as a function of column density and scale. On the other hand we stressed that this cirrus noise estimate relies on the hypothesis of Gaussian fluctuations, which is clearly not the case for interstellar emission. In that context we proposed a method to modify Gaussian random fields such that it reproduces the power spectrum but also the level of non-Gaussianity observed which is related to the fact that bright regions have stronger brightness fluctuations than faint ones. Such images could be used to tests component separation algorithms (including point source extraction) that have to deal with non-Gaussian components. The main limitation of the technique we propose is that it does not reproduce the obvious filamentarity seen in observations.

Some of the results in this paper have been obtained using the HEALPix package (Gorski et al., 2005). This work

was supported by the Canadian Space Agency. It is a pleasure to thank J. Richard Bond for enlightening discussions.

References

Abergel, A., Boulanger, F., Delouis, J. M., Dudziak, G. & Steindling, S. 1996, *A&A*, 309, 245.

Aghanim, N., Kunz, M., Castro, P. G. & Forni, O. 2003, *A&A*, 406, 797–816.

Audit, E. & Hennebelle, P. 2005, *A&A*, 433, 1–13.

Bazell, D. & Desert, F. X. 1988, *ApJ*, 333, 353.

Bensch, F., Stutzki, J. & Ossenkopf, V. 2001, *A&A*, 366, 636.

Bernard, J. P., Abergel, A., Ristorcelli, I., Pajot, F., Torre, J. P., Boulanger, F., Giard, M., Lagache, G., Serra, G., Lamarre, J. M., Puget, J. L., Lepeintre, F. & Cambrésy, L. 1999, *A&A*, 347, 640.

Boulanger, F. & Péault, M. 1988, *ApJ*, 330, 964.

Boulanger, F., Abergel, A., Bernard, J. P., Burton, W. B., Desert, F. X., Hartmann, D., Lagache, G. & Puget, J. L. 1996, *A&A*, 312, 256.

Brunt, C. M. & Heyer, M. H. 2002, *ApJ*, 566, 276.

Brunt, C. M. 2003, *ApJ*, 583, 280.

Crovisier, J. & Dickey, J. M. 1983, *A&A*, 122, 282.

Desert, F. X., Boulanger, F. & Puget, J. L. 1990, *A&A*, 237, 215.

Dickey, J. M., McClure-Griffiths, N. M., Stanimirovic, S., Gaensler, B. M. & Green, A. J. 2001, *ApJ*, 561, 264.

Dickman, R. L., Margulis, M. & Horvath, M. A. 1990, *ApJ*, 365, 586.

Elmegreen, B. G., Kim, S. & Staveley-Smith, L. 2001, *ApJ*, 548, 749.

Elmegreen, B. G. 2002, *ApJ*, 564, 773.

Falgarone, E., Phillips, T. G. & Walker, C. K. 1991, *ApJ*, 378, 186.

Finkbeiner, D. P., Davis, M. & Schlegel, D. J. 1999, *ApJ*, 524, 867.

Gautier, T. N. I., Boulanger, F., Perault, M. & Puget, J. L. 1992, *AJ*, 103, 1313.

Goldman, I. 2000, *ApJ*, 541, 701.

Gorski, K. M., Hivon, E., Banday, A. J., Wandelt, B. D., Hansen, F. K., Reinecke, M. & Bartelmann, M. 2005, *ApJ*, 622, 759–771.

Green, D. A. 1993, *MNRAS*, 262, 327.

Hauser, M. G., Arendt, R. G., Kelsall, T., Dwek, E., Odegard, N., Weiland, J. L., Freudenreich, H. T., Reach, W. T., Silverberg, R. F., Moseley, S. H., Pei, Y. C., Lubin, P., Mather, J. C., Shafer, R. A., Smoot, G. F., Weiss, R., Wilkinson, D. T. & Wright, E. L. 1998, *ApJ*, 508, 25–43.

Helou, G. & Beichman, C. A. The confusion limits to the sensitivity of submillimeter telescopes. In ESA, editor, *From Ground-Based to Space-Borne Sub-mm Astronomy*, page 117, 1990.

Hobson, M. P. 1992, *MNRAS*, 256, 457.

Ingalls, J. G., Miville-Deschénes, M. A., Reach, W. T., Noriega-Crespo, A., Carey, S. J., Boulanger, F., Stolovy, S. R., Padgett, D. L., Burgdorf, M. J., Fajardo-Acosta, S. B., Glaccum, W. J., Helou, G., Hoard, D. W., Karr, J., O'Linger, J., Rebull, L. M., Rho, J., Stauffer, J. R. & Wachter, S. 2004, *Astrophysical Journal Supplement Series*, 154, 281–285.

Jeong, W. S., Mok Lee, H., Pak, S., Nakagawa, T., Minn Kwon, S., Pearson, C. P. & White, G. J. 2005, *MNRAS*, 357, 535–547.

Jewell, J. 2001, *ApJ*, 557, 700.

Joncas, G., Boulanger, F. & Dewdney, P. E. 1992, *ApJ*, 397, 165.

Kiss, C., Abraham, P., Klaas, U., Lemke, D., Heraudeau, P., Burgo, C. D. & Herbster, U. 2003, *A&A*, 399, 177.

Lagache, G., Haffner, L. M., Reynolds, R. J. & Tufte, S. L. 2000, *A&A*, 354, 247.

Li, A. & Draine, B. T. 2001, *ApJ*, 554, 778–802.

Miville-Deschénes, M. A. & Lagache, G. 2005, *Astrophysical Journal Supplement Series*, 157, 302–323.

Miville-Deschénes, M. A., Lagache, G. & Puget, J. L. 2002, *A&A*, 393, 749.

Miville-Deschénes, M. A., Joncas, G., Falgarone, E. & Boulanger, F. 2003a, *A&A*, 411, 109.

Miville-Deschénes, M. A., Levrier, F. & Falgarone, E. 2003b, *ApJ*, 593, 831.

Padoan, P., Rosolowsky, E. W. & Goodman, A. A. 2001, *ApJ*, 547, 862.

Padoan, P., Cambrésy, L. & Langer, W. 2002, *ApJ*, 580, L57.

Padoan, P., Goodman, A. A. & Juvela, M. 2003, *ApJ*, 588, 881.

Padoan, P., Cambrésy, L., Juvela, M., Kritsuk, A., Langer, W. D. & Norman, M. L. 2006, *ApJ*, 649, 807–815.

Rocha, G., Hobson, M. P., Smith, S., Ferreira, P. & Challinor, A. 2005, *MNRAS*, 357, 1–11.

Stanimirovic, S. & Lazarian, A. 2001, *ApJ*, 551, L53.

Stanimirovic, S., Staveley-Smith, L., Dickey, J. M., Sault, R. J. & Snowden, S. L. 1999, *MNRAS*, 302, 417.

Starck, J. L. & Murtagh, F. 1998, *Publications of the Astronomical Society of the Pacific*, 110, 193.

Stepnik, B., Abergel, A., Bernard, J. P., Boulanger, F., Cambrésy, L., Giard, M., Jones, A. P., Lagache, G., Lamarre, J. M., Meny, C., Pajot, F., Peintre, F. L., Ristorcelli, I., Serra, G. & Torre, J. P. 2003, *A&A*, 398, 551.

Stutzki, J., Bensch, F., Heithausen, A., Ossenkopf, V. & Zielinsky, M. 1998, *A&A*, 336, 697.

Vio, R., Andreani, P. & Wamsteker, W. 2001, *Publications of the Astronomical Society of the Pacific*, 113, 1009–1020.

Vio, R., Andreani, P., Tenorio, L. & Wamsteker, W. 2002, *Publications of the Astronomical Society of the Pacific*, 114, 1281–1289.

Vogelaar, M. G. R. & Wakker, B. P. 1994, *A&A*, 291, 557.

Wright, E. L. 1998, *ApJ*, 496, 1.